ACS APPLIED ENERGY MATERIALS

www.acsaem.org Article

Rationally Engineered Ultrastable Three-Dimensional (3D) Conjugated Microporous Polymers Containing Triptycene, Tetraphenylethene, and Benzothiadiazole Units as Exceptional High-Performance Organic Electrodes for Supercapacitors

Tzu-Hsin Weng, Mohamed Gamal Mohamed,* Santosh U. Sharma, Islam M. A. Mekhemer, Ho-Hsiu Chou, and Shiao-Wei Kuo*

Cite This: *ACS Appl. Energy Mater.* 2023, 6, 9012−9024 Read Online

ACCESS | Metrics & More | Article Recommendations | Supporting Information

ABSTRACT: Conjugated microporous polymers (CMPs) have been investigated as promising materials for enhancing energy storage in supercapacitors. Supercapacitors can be categorized into electric double-layer capacitors (EDLC) and pseudocapacitors, each differing in how their electrodes interact with ions. In the process of synthesizing CMPs, four specific building blocks, namely, triptycene (Try), pyrene (Py), tetraphenylethene (TPE), and benzo[*c*][1,2,5]thiadiazole (BT), were utilized. To synthesize Try-PyT CMP, Try-PyT-BT CMP, Try-TPET CMP, and Try-TPET-BT CMP, an efficient and environmentally friendly synthesis method was employed. This technique involved a one-pot Sonogashira coupling reaction. The analysis phase encompassed a range of assessments, including Fourier transform infrared (FTIR) spectroscopy, thermogravimetric analysis (TGA), ^{13}C solid-state NMR, scanning electron microscopy (SEM), transmission electron microscopy (TEM), N_2 adsorption/desorption isotherm measurements, cyclic voltammetry (CV), and galvanostatic charge−discharge (GCD). These analyses were performed to evaluate the chemical structures, thermal stability, porosity, morphology, and electrochemical properties of the four CMPs based on Try. The study highlighted the exceptional performance of these Try-based CMPs as electrode materials for supercapacitors. In particular, the Try-TPET-BT CMP demonstrated an impressive capacitance of 157 F g^{-1} at 0.5 A g^{-1}, coupled with remarkable stability across 2000 cycles. Their substantial surface area and pore volume make them strong contenders for practical applications in real-world devices.

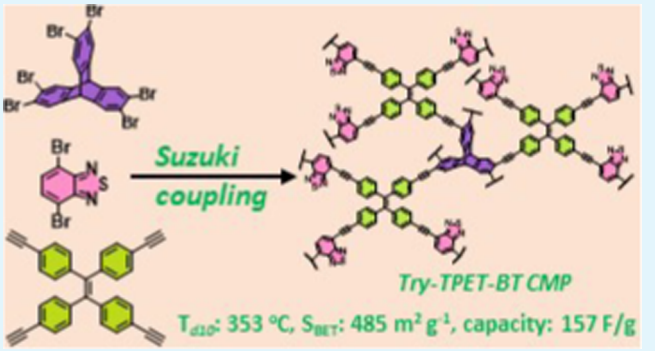

KEYWORDS: *triptycene, tetraphenylethene, benzo[c][1,2,5]thiadiazole, Sonogashira coupling, conjugated microporous polymers, supercapacitor*

INTRODUCTION

Porous organic polymers (POPs) could be synthesized from several organic routes such as Suzuki coupling (organoboronic acid and halides), Sonogashira (carbon−carbon bond between a terminal alkyne and an aryl or vinyl halide), Heck (aryl halides or vinyl halides and activated alkenes), and others.[1−15] POPs could have some potential applications including gas storage and separation, energy storage such as supercapacitors and batteries, catalysis, sensing, drug delivery, and water purifications.[16−25] Compared with the covalent organic frameworks (COFs) and metal−organic frameworks (MOFs) with highly crystalline properties as well as extensively developed materials, conjugated microporous polymers (CMPs) are a kind of amorphous polymer with a unique π-electron conjugated skeleton. The rich π-electron on the conducting polymers results in the comprehensive exhibition of electrical, optical, and magnetic properties. Above and beyond, the amorphous property allows the monomer choice more flexible to diverse the network and has attracted attention in science research and industry applications.[26−33]

Triptycene (Try) is aromatic hydrocarbon with three benzene rings fused together in a triangular shape, and the central benzene ring is perpendicular to the other two benzene rings forming a three-dimensional (3D) structure with D_{3h} symmetry, three outside benzene rings including 120° make triptycene be a concaved shape structure, it absolutely prevents

Received: August 3, 2023
Accepted: August 18, 2023
Published: August 30, 2023

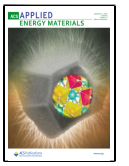

https://doi.org/10.1021/acsaem.3c01933
ACS Appl. Energy Mater. 2023, 6, 9012−9024

the packing of planar properties monomer. In this study, the hexa-functionalized triptycene monomer is synthesized through bromination on the carbons with 2, 3, 6, 7, 14, and 15, and the highly dense arrangement of six functionalities could be as maximum as possible to increase the cross-link density as well as increase the surface area. Since the first triptycene structure was published in 1942, there have already been a lot of studies taking this compound into account.[34] For instance, triptycene's inherent symmetry and concave structure make it a prime candidate for incorporation into macrocyclic arenes. Its electron-rich cavity bestows upon it a unique chemical architecture, endowing it with host−guest interactions, responsiveness to stimuli, and the capacity for self-assembly. On the other hand, combined with the flexibility of monomers in POPs, the three-dimensional property of triptycene is well designed as a building unit.[35−43] For example, Ghanem et al. published the first POP containing triptycene unit,[44] and then, a series of triptycene-based POPs were reported in recent years. Benefiting from the extensive functional sites, Fang et al. synthesized a 3D stp-topologized COFs with a porphyrin or metalloporphyrin building unit.[45] In addition, Fu et al. have reported the different functional POSS such as (T_8, T_{10}, and T_{12}) units with the triptycene components to form organic/inorganic hybrid POPs.[46]

Energy density, power capacity, and long cycle stability are essential requirements for an electrode material in energy storage devices. Considering these three factors, we inserted a highly functional unit into a network structure to be a new material and made it a component of an energy storage device.[47,48] Basically, energy storage devices could be separated into two major classes (battery and supercapacitor), and then there are two subclasses of supercapacitors (EDLC and pseudocapacitors). Furthermore, by leveraging the advantages of the aforementioned subclasses, numerous studies have proposed innovative strategies to endow materials with dual characteristics.[49,50] In this work, a series of four different composite materials (CMPs) were synthesized by using a quick and low-waste approach. These CMPs were composed of Try, Py, TPE, and BT moieties. The synthesis method involved a one-pot Sonogashira coupling process. The four CMPs synthesized were Try-PyT CMP, Try-PyT-BT CMP, Try-TPET CMP, and Try-TPET-BT CMP. To characterize these Try-based CMPs, various analytical techniques were employed. Chemical composition analysis was performed by using Fourier transform infrared (FTIR) and solid-state NMR spectroscopy. Thermal stability was evaluated using thermogravimetric analysis (TGA). The porosity and surface morphology of the Try-based CMPs were examined using scanning electron microscopy (SEM) and transmission electron microscopy (TEM), respectively. The N_2 adsorption/desorption isothermal measurements were conducted to determine the porosity of the CMPs linked Try units. Additionally, electrochemical measurements were performed to evaluate the suitability of these Try-based CMPs as supercapacitor electrode materials. Cyclic voltammetry (CV) and galvanostatic charge−discharge (GCD) studies were conducted. The Try-TPET-BT CMP exhibited the highest capacitance value of 157 F g^{-1} at 0.5 A g^{-1} and demonstrated excellent stability over 2000 cycles. Overall, the rigid cross-linked networks with high bonding energy of triple bond achieve a strong and stable material structure and the heteroatom (N, S) afforded by BT unit expands the energy density for Try-based CMPs.[51−56]

EXPERIMENTAL SECTION

Materials. Triptycene (Try, 98%), bromine (Br_2), copper(I) iodide (CuI, 99.5%), triphenylphosphine (PPh_3, 99%), titanium tetrachloride ($TiCl_4$, 99.9%), 99.9%, anhydrous magnesium sulfate ($MgSO_4$, 99.5%), dimethylformamide (DMF), methanol (MeOH), dichloromethane (DCM), tetrakis(triphenylphosphine) palladium(0) [$Pd(PPh_3)_4$], and triethylamine (Et_3N, 99.5%) were purchased from Alfa Aesar and Sigma-Aldrich. In accordance with our earlier investigations, we effectively prepared the precursors essential for synthesizing 1,3,6,8-tetrakis(2-(trimethylsilyl)ethynyl)pyrene (PyT-Si_4) and 1,1,2,2-tetrakis(4-((trimethylsilyl)ethynyl)phenyl)ethane (TPET-Si_4).[57−62]

Synthesis of 2,3,6,7,14,15-Hexabromotriptycene (Try-Br_6). $CHCl_3$ was combined with Try (4.00 g, 15.6 mmol), I_2 (0.52 g, 1.60 mmol), Fe (0.320 g, 5.6 mmol), and Br_2 (2.80 mL, 156.0 mmol), which was then heated at 65 °C for 24 h. Excess $CHCl_3$ was then evaporated under a decreased pressure after cooling to ambient temperature. A white powder was produced by purifying the crude materials using column chromatography with hexane as the eluent (yield: 80%; $T_m \geq$ 350 °C). FTIR: 3071, 2928 (Figure S1). ^{1}H NMR (Figure S2): 7.61, 5.23 (CH aliphatic). ^{13}C NMR (Figure S3): 144.37, 129.54, 122.99, 51.30 (aliphatic carbon nuclei). T_{d10} = 461 °C and char yield = 4 wt % (by TGA).

Synthesis of 1,3,6,8-Tetraethynyl-4,6-dihydropyrene (PyT). PyT-Si_4 (6.4 g, 10.4 mmol) and K_2CO_3 (11.24 g, 81.6 mmol) were dissolved in 150 mL of MeOH and agitated at room temperature for 48 h. Brown solids were produced after K_2CO_3 had been taken out of the crude products using a water wash. FTIR (Figure S4): 3268 (≡C−H), 2118. ^{1}H NMR (Figure S5): 7.24, 6.93, 3.06 (≡C−H). ^{13}C NMR (Figure S6): 143.8−121.24, 83.6 (≡C−Ar), 77.88 (≡C−H).

Synthesis of 1,1,2,2-Tetrakis(4-ethynylphenyl)ethene (TPET). TPET-Si_4 (6.4 g, 10.8 mmol) and K_2CO_3 (11.24 g, 81.6 mmol) were combined with 100 mL of MeOH and agitated for 48 h at room temperature. The crude products were washed with water to remove K_2CO_3 and yield a yellow solid. FTIR (Figure S7): 3255 (≡C−H), 2168 (C≡C). ^{1}H NMR (Figure S8): 7.24, 6.93, 3.1 (≡C−H). ^{13}C NMR (Figure S9): 143.8−121.24, 83.6, 77.88 (≡C−H).

Synthesis of 4,7-Dibromobenzo[c][1,2,5]thiadiazole (BT-Br_2). Benzo[*c*][1,2,5]thiadiazole (20.0 g, 293.6 mmol), HBr (48%), and Br_2 solution were combined, and the resulting mixture was refluxed at 100 °C for 24 h. The BT-Br_2 solution was prepared by adding DCM after the addition of the NaOH solution at 0 °C. The solvent was then extracted under decreased pressure to get the final white powder (10 g, 50%). FTIR (Figure S10): 3035 cm^{-1}. ^{1}H NMR (Figure S11): 7.74 ppm. ^{13}C NMR (Figure S12): 154−115 ppm.

Synthesis of Try-PyT, Try-PyT-BT, Try-TPET, and Try-TPET-BT CMPs. To prepare the Try-PyT CMP, Try-Br_6 (0.4 g), PyT (0.05 g), PPh_3 (0.07 g), $Pd(PPh_3)_4$ (0.06 g), and CuI (0.07 g) were dissolved in 40 mL of Et_3N and DMF under the degassed condition and heated to 110 °C for 3 days to provide a red precipitate solid [Scheme S1]. To synthesize Try-PyT-BT CMP as a red solid [Scheme S2], Try-Br_6 (0.4 g), PyT (0.05 g), and BT-Br_2 (0.01 g) were used. To prepare Try-TPET CMP as a brown solid [Scheme S3], Try-Br_6 (0.4 g) and TPET (0.5 g) were used. To prepare Try-TPET-BT CMP as a brown solid [Scheme S4], Try-Br_6 (0.4 g), TPET (0.05 g), and BT-Br_2 (0.01 g) were used. All produced Try-CMPs in this study were produced by THF, MeOH, and acetone.

RESULTS AND DISCUSSION

Syntheses and Characterizations of Try-Based CMPs [Try-PyT, Try-PyT-BT, Try-TPET, and Try-TPET-BT CMPs]. To produce Try-CMPs, a combination of two or more monomers is essential. The choice of monomers is crucial and depends on the synthesis route as well as the selective functional groups present in these monomers. Here are four specific monomers provided for this purpose: Try-Br_6, this monomer is synthesized by performing a bromination reaction on triptycene; BT-Br_2 is obtained through a bromination

https://doi.org/10.1021/acsaem.3c01933
ACS Appl. Energy Mater. 2023, 6, 9012−9024

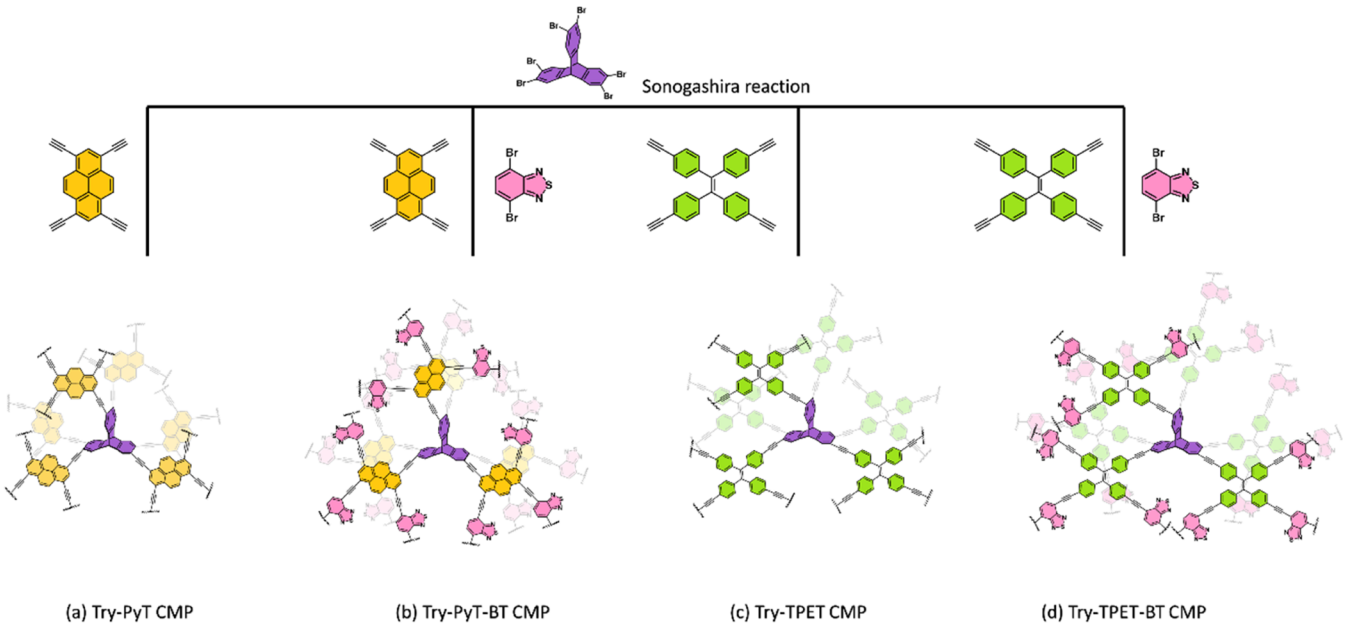

Figure 1. Synthesis of four triptycene (Try)-based CMPs including (a) Try-PyT CMP, (b) Try-PyT-BT CMP, (c) Try-TPET CMP, and (d) Try-TPET-BT CMP.

reaction on benzo[*c*][1,2,5]thiadiazole;[62] PyT and TPET were synthesized by removing the terminal trimethylsilane groups in the presence of K_2CO_3 and MeOH. Additionally, two important monomers, tetraphenylethene (TPE) and pyrene (Py), are widely used in the design of organic luminescent materials and optoelectronic devices.[63−65] TPE is commonly employed in organic luminescent materials due to its central ethylene double bond, which makes it prone to undergo photoinduced isomerization frequently. This property is advantageous in luminescent applications. On the other hand, the Py molecule possesses four benzene rings fused together, resulting in an extensive π-electron system.[65] The optical and structural characteristics of pyrene make it highly valuable in various optoelectronic devices. Due to the unique properties of pyrene and TPE, both molecules have found extensive use in the field of optoelectronics, contributing to the development of various devices in this domain.[63−67]

Sonogashira and Hagihara et al. have reported a new coupling synthesis route, and this approach has been widely used to prepare organic porous polymers with conjugated skeleton through this reaction.[68] This is a cross-coupling reaction that is found in organic synthesis to form a strong triple bond between an aryl or vinyl halide and a terminal alkyne. In this study, we prepared four different Try-CMPs using the following monomer combinations: Try-Br_6 with PyT, PyT/BT-Br_2, TPET, and TPET/BT-Br_2. We utilized the Sonogashira reaction in the presence of EtN_3 under moderate conditions at 90 °C for 3 days to facilitate the polymerization process. The resulting CMPs were collected as dark red solids in relatively high yields. Specifically, the Try-PyT CMP and Try-PyT-BT CMP were obtained from the central unit Try-Br_6 combined with PyT and PyT/BT-Br_2 mixture, respectively, as depicted in Figure 1a,b. The yields for Try-PyT CMP and Try-PyT-BT CMP were 78 and 82%, respectively. Furthermore, the Try-TPET CMP and Try-TPET-BT CMP were synthesized as brown solids. These CMPs were derived from Try-Br_6 as the central unit, combined with TPET and TPET/BT-Br_2 mixture, respectively, as illustrated in Figure 1c,d. The yields for Try-TPET CMP and Try-TPET-BT CMP were 75 and 80%, respectively. Overall, the successful synthesis of these four Try-based CMPs using the Sonogashira reaction under moderate conditions demonstrates the feasibility of this approach in creating porous polymers with conjugated structures. The obtained Try-CMPs hold promise for potential applications in energy storage fields due to their specific compositions and properties. These four Try-based CMPs exhibit a high degree of polymerization and cross-linking density, as evidenced by their insolubility in both water and various organic solvents, such as THF, DMF, methanol, $CHCl_3$, and acetone.

The confirmation of their chemical structures was carried out using FTIR (Fourier transform infrared) spectroscopy and ^{13}C solid-state CP/MAS NMR spectroscopy. FTIR analysis of Try-Br_6 revealed absorption peaks at approximately 2924 and 3060 cm^{-1}, corresponding to aliphatic CH and aromatic CH groups, respectively (Figure 2). PyT and TPET exhibited characteristic absorption peaks for triple bonds (≡C−H and C≡C) at 3283, 3272, 2198, and 2105 cm^{-1}, respectively. BT-Br_2 showed absorption peaks for C−Br at 586 cm^{-1}, aromatic CH at 3078 and 3045 cm^{-1}, and aromatic C═C at 1586 cm^{-1}. In all Try-based CMPs, the C≡C−H absorptions at 3283 and 3272 cm^{-1} disappeared due to the formation of the cross-linked structure during the Sonogashira reaction. However, the C≡C absorptions remained, indicating the presence of internal C≡C structures in the Try-CMPs. These internal C≡C absorptions were slightly shifted to 2100 cm^{-1} for Try-PyT CMP, 2181 cm^{-1} for Try-PyT-BT CMP, 2195 cm^{-1} for Try-TPET CMP, and 2200 cm^{-1} for Try-TPET-BT CMP, compared to monomers PyT (at 2198 cm^{-1}) and TPET (at 2105 cm^{-1}). This shift indicates the successful formation of these Try-based CMPs. Furthermore, the C−Br absorption at 586 cm^{-1} from BT-Br_2 disappeared in Try-PyT-BT CMP and Try-TPET-BT CMP, and new absorption peaks emerged within the ranges of 3133−3029 cm^{-1} (aromatic CH), 2955−2930 cm^{-1} (aliphatic CH), and 1620−1550 cm^{-1} (aromatic C═C). These results provide further evidence for the

https://doi.org/10.1021/acsaem.3c01933
ACS Appl. Energy Mater. 2023, 6, 9012−9024

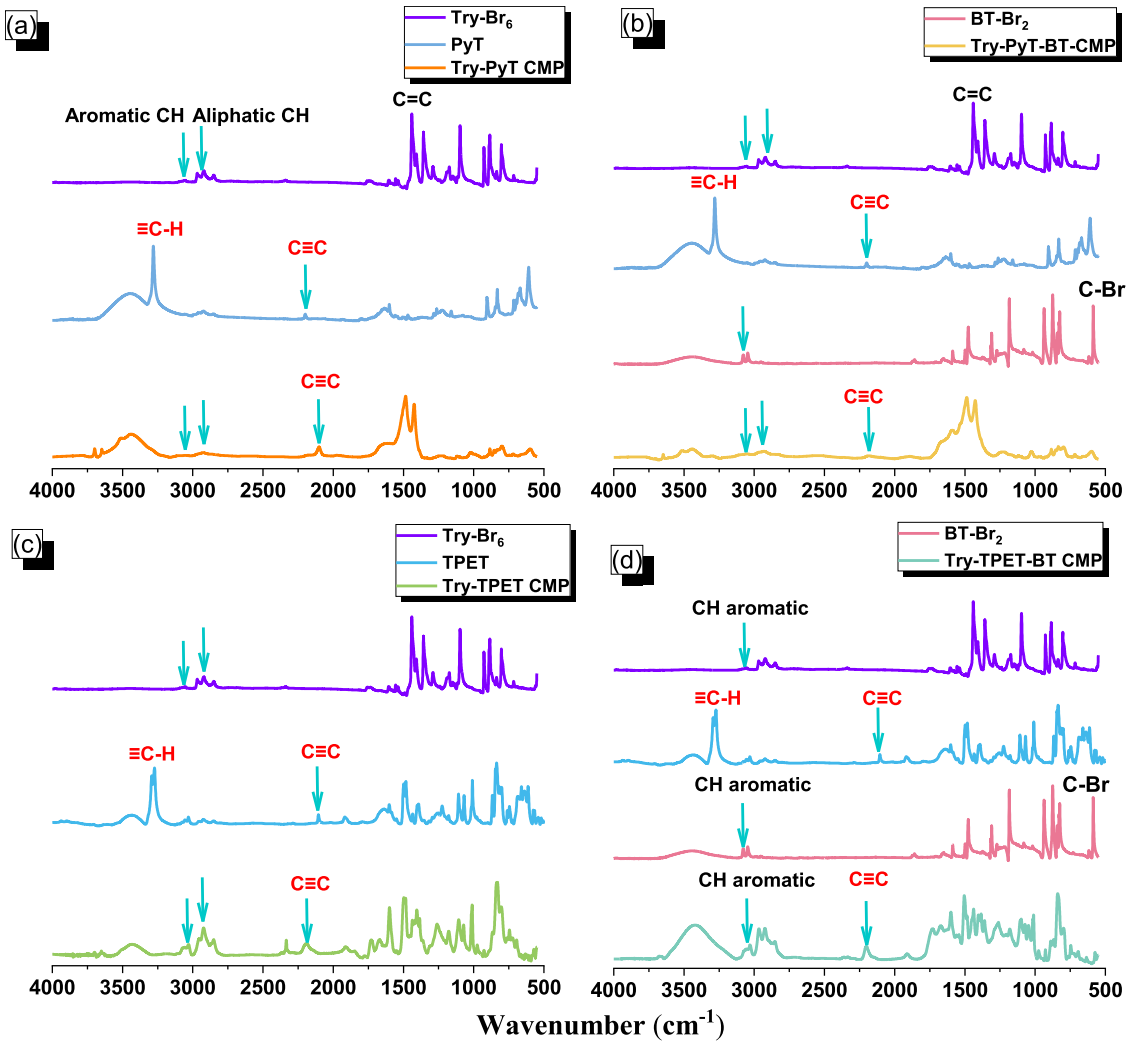

Figure 2. FTIR spectra of the corresponding monomers and Try-CMPs of (a) Try-PyT, (b) Try-PyT-BT, (c) Try-TPET, and (d) Try-TPET-BT CMPs.

successful formation of all four Try-based CMPs, as indicated by the FTIR analyses shown in Figure 2.

Figure 3 shows the corresponding ^{13}C solid-state CP/MAS NMR spectra of the four Try-based CMPs. As expected, the cross-linked structures of these CMPs could not be dissolved in any organic solvents due to their high degree of polymerization and cross-linking density. The NMR spectra reveal distinct carbon signals, providing valuable insights into the composition of these CMPs. The signals appearing in the range of 147.20−111.26 ppm are attributed to aromatic carbons, indicating the presence of aromatic rings within the framework of the CMPs. Notably, signals at 81.65−80.63 ppm correspond to the internal C≡C moieties, confirming the successful incorporation of the triple bond units within the CMPs. These internal C≡C signals are likely to arise from the reaction of Try with PyT or TPET during the Sonogashira coupling, leading to the formation of the cross-linked structures. Furthermore, signals at 54.96−52.11 ppm are assigned to aliphatic CH units originating from the Try group, providing additional evidence of the successful integration of Try moieties within the CMP frameworks.[28] Taken together, the ^{13}C solid-state CP/MAS NMR spectra support the successful incorporation of both tryptophan and C≡C moieties into the structures of these four Try-based CMPs, confirming their well-defined and cross-linked frameworks. These findings further validate the feasibility of the Sonogashira reaction approach in synthesizing highly structured and stable Try-based CMPs.

To understand the thermal stability of these Try-based CMPs, we used TGA under a N_2 atmosphere from 100 to 800 °C, and all Try-based CMPs exhibited good thermal stability, as shown in Figure 4 and also summarized in Table 1. The T_{d10} values of Try-PyT, Try-PyT-BT, Try-TPET, and Try-TPET-BT CMPs are at 366, 304, 399, and 353 °C, and the char yields after heating to 800 °C were 67, 60, 70, and 60 wt %, respectively. The results of the TGA clearly show that Try-PyT and Try-TPET CMPs exhibit better thermal stability compared to Try-PyT-BT and Try-TPET-BT CMPs. This observation suggests that the incorporation of the BT monomer into Try-PyT and Try-TPET CMPs may lead to a reduction in cross-linking density, resulting in longer construction skeletons, as we had anticipated. As a consequence, the thermal stability of Try-PyT-BT and Try-TPET-BT CMPs is slightly decreased compared to the other two CMPs.

The porous properties of the four Try-based CMPs were investigated through N_2 adsorption and desorption measurements at 77 K. The BET model was employed to calculate

https://doi.org/10.1021/acsaem.3c01933
ACS Appl. Energy Mater. 2023, 6, 9012−9024

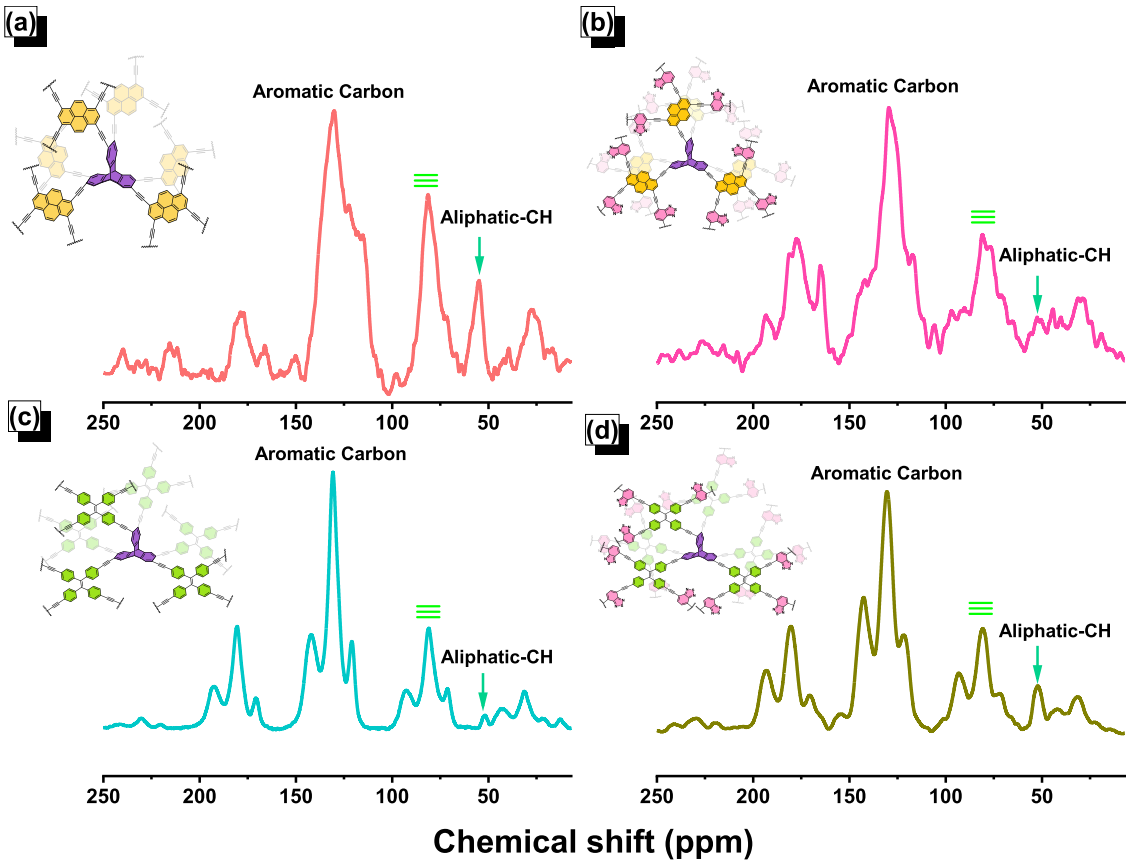

Figure 3. ^{13}C CP/MAS solid-state NMR spectra of (a) Try-PyT, (b) Try-PyT-BT, (c) Try-TPET, and (d) Try-TPET-BT CMPs.

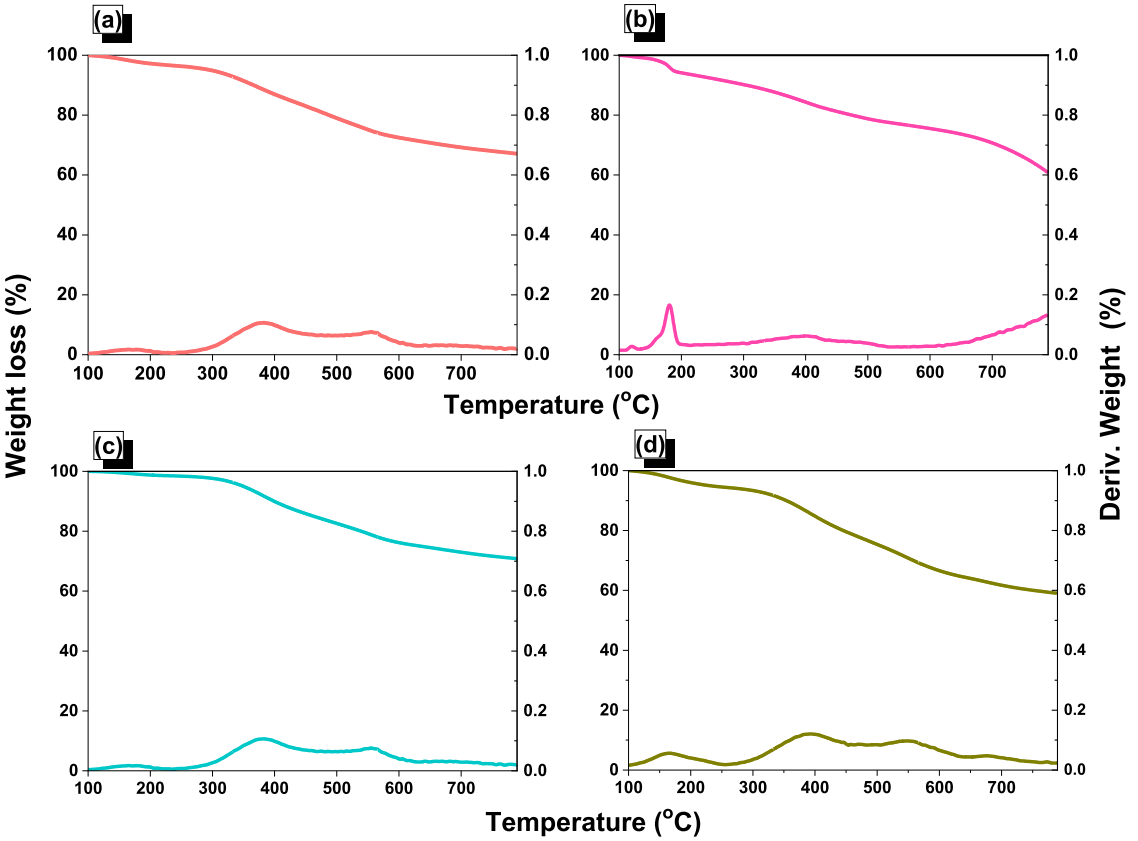

Figure 4. TGA traces of the (a) Try-PyT, (b) Try-PyT-BT, (c) Try-TPET CMPs, and (d) Try-TPET-BT CMPs.

https://doi.org/10.1021/acsaem.3c01933
ACS Appl. Energy Mater. 2023, 6, 9012−9024

Table 1. TGA, Brunauer–Emmett–Teller (BET), and Capacitance Data of 3D Try-CMPs

sample	T_{d10} (°C)	char yield (wt %)	surface area (m^2 g^{-2})	pore size (nm)	capacity (F g^{-1})
Try-PyT CMP	366	67	613	1.02	66
Try-PyT-BT CMP	304	60	402	1.29	116
Try-TPET CMP	399	70	601	1.29	100
Try-TPET-BT CMP	353	60	485	1.06	157

their surface area, pore volume, and pore diameter, as illustrated in Figure 5 and Table 1. The total pore volumes were determined from the N_2 isotherm at $P/P_0 = 0.99$, and the pore size distribution curves were obtained by using the nonlocal density functional theory (NLDFT) method. Analysis of the N_2 adsorption/desorption isothermal curves revealed that all four Try-based CMPs exhibited a combination of Type I and Type IV isotherms as per the IUPAC classification. This suggested the presence of a micro/mesoporous structure in these materials. The rapid N_2 adsorption uptake observed at both relatively lower and higher pressures further supported this conclusion. During the desorption process of the Try-PyT, Try-TPET, and Try-TPET-BT CMPs, a slight hysteresis phenomenon was observed. This behavior can be attributed to the coexistence of micro- and mesopores within the materials. The surface area and pore volume were calculated to be 613 m^2 g^{-1} and 0.61 cm^3 g^{-1} for Try-PyT CMP; 402 m^2 g^{-1} and 0.49 cm^3 g^{-1} for the Try-PyT-BT CMP; 601 m^2 g^{-1} and 0.68 cm^3 g^{-1} for the Try-TPET CMP; and 485 m^2 g^{-1} and 0.73 cm^3 g^{-1} for the Try-TPET-BT CMP. Next, the pore diameter distribution of CMPs was Try-PyT (1.02 and 1.78 nm), Try-PyT-BT (1.29 nm and 1.83), Try-TPET (1.29 and 1.92 nm), and Try-TPET-BT (1.06 and 1.79 nm), suggesting four CMPs featuring micro/mesoporous behavior. Furthermore, in agreement with the TGA results, the incorporation of the BT unit led to a decrease in the surface areas of Try-PyT CMP and Try-TPET-BT CMP compared to those of their counterparts without the BT unit.

Field emission scanning electron microscopy (SEM) revealed that all four Try-based CMPs displayed irregular shapes and exhibited a tendency to aggregate together, as depicted in Figure 6a–d. The elemental composition was confirmed by energy-dispersive spectroscopy (EDS). Try-PyT CMP and Try-TPET CMP showed the presence of only carbon atoms, represented by the red color in the EDS analysis. On the other hand, Try-PyT-BT CMP and Try-TPET-BT CMP exhibited the presence of additional nitrogen and sulfur atoms, indicated by the white and green colors, respectively, as shown in Figures S13–S16. For further

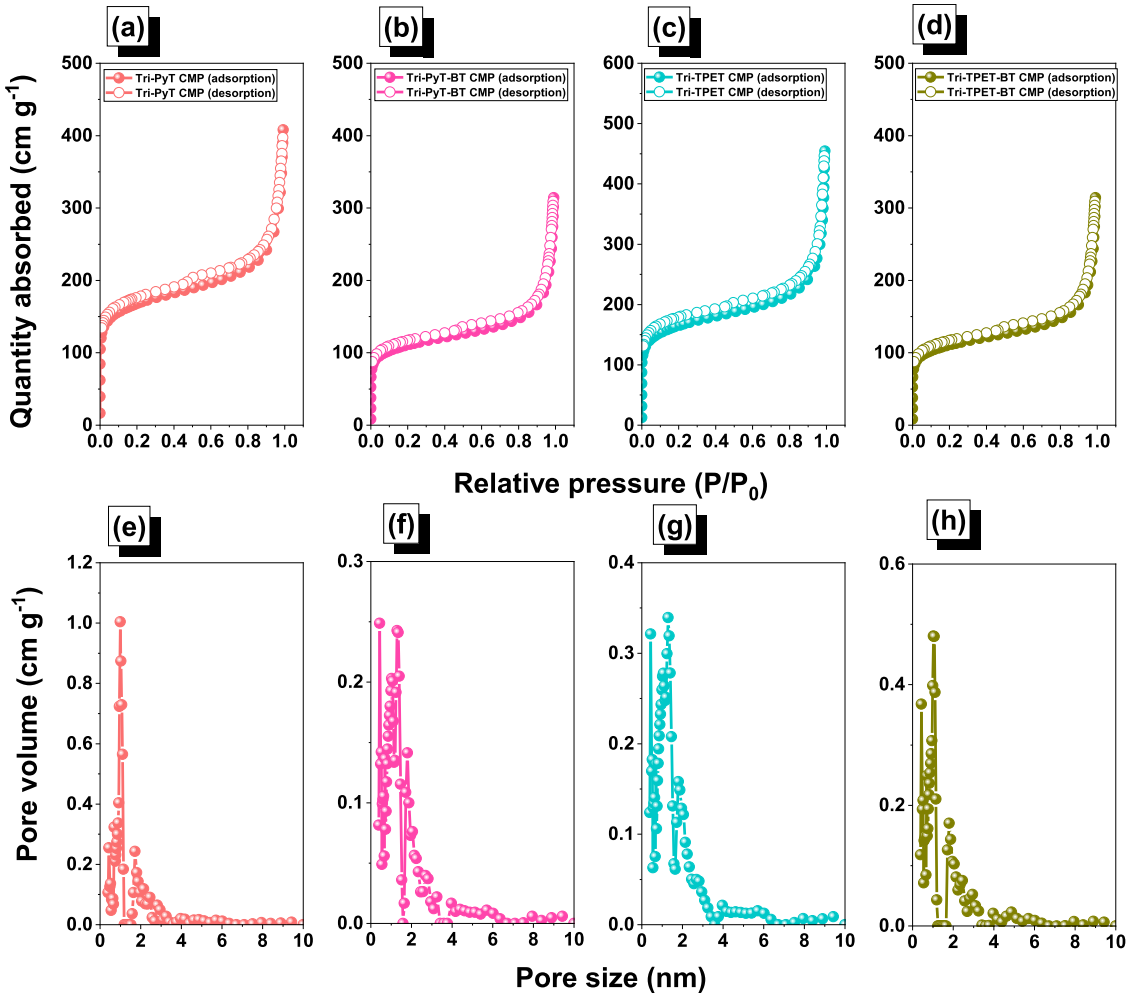

Figure 5. (a–d) N_2 adsorption/desorption isotherms and (e–h) pore size distributions of the (a, e) Try-PyT, (b, f) Try-PyT-BT, (c, g) Try-TPET, and (d, h) Try-TPET-BT CMPs.

https://doi.org/10.1021/acsaem.3c01933
ACS Appl. Energy Mater. 2023, 6, 9012–9024

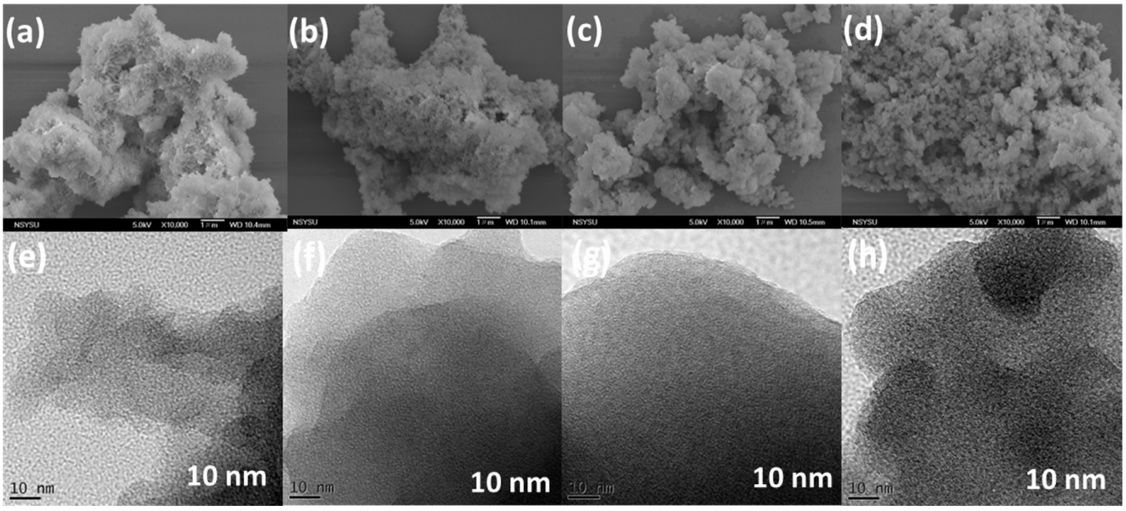

Figure 6. SEM and TEM images of the (a, e) Try-PyT, (b, f) Try-PyT-BT, (c, g) Try-TPET, and (d, h) Try-TPET-BT CMPs.

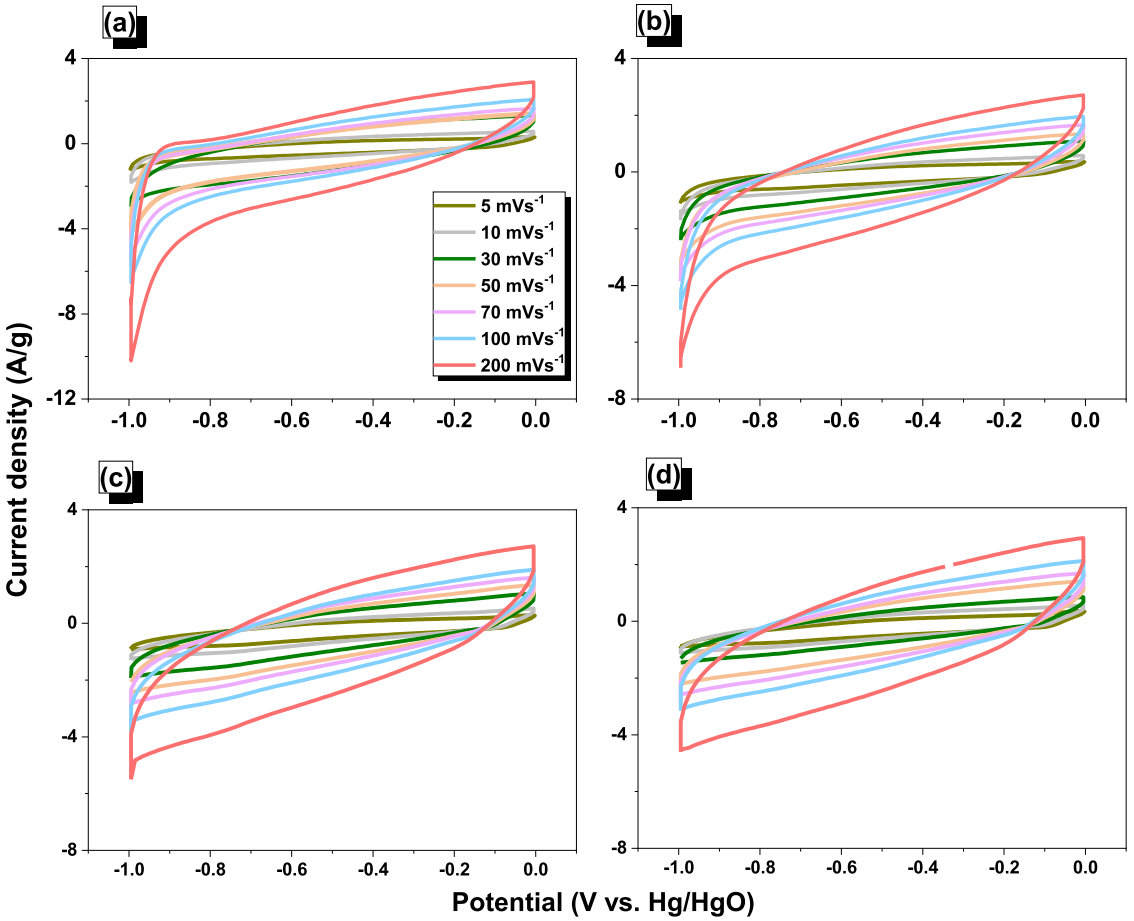

Figure 7. (a–d) CV curves of the (a) Try-PyT, (b) Try-PyT-BT, (c) Try-TPET, and (d) Try-TPET-BT CMPs.

investigation, transmission electron microscopy (TEM) analyses were conducted on these Try-based CMPs [Figure 6e–h]. The TEM results revealed that these materials lacked an orderly pore arrangement, suggesting that they possessed amorphous structures with irregularly shaped pores.

Electrochemical Performance of the Try-Based CMPs. The current response of Try-based CMPs was investigated through cyclic voltammetry (CV) at various scan rates, including 5, 10, 30, 50, 70, 100, and 200 mV s^{-1}. The CV measurements revealed that all four Try-based CMP electrodes exhibited quasi-rectangular shapes with a slightly embedded redox peak, as illustrated in Figure 7a–d. This observation suggests that these four electrodes possess a combination of properties characteristic of both an electrostatic double-layer capacitor (EDLC) and a pseudocapacitor.

Furthermore, Figure 8a–d presents the results of galvanostatic charge–discharge (GCD) tests conducted at a range of current densities, specifically 0.5, 1, 2, 3, 5, 7, 10, 15, and 20 A

https://doi.org/10.1021/acsaem.3c01933
ACS Appl. Energy Mater. 2023, 6, 9012–9024

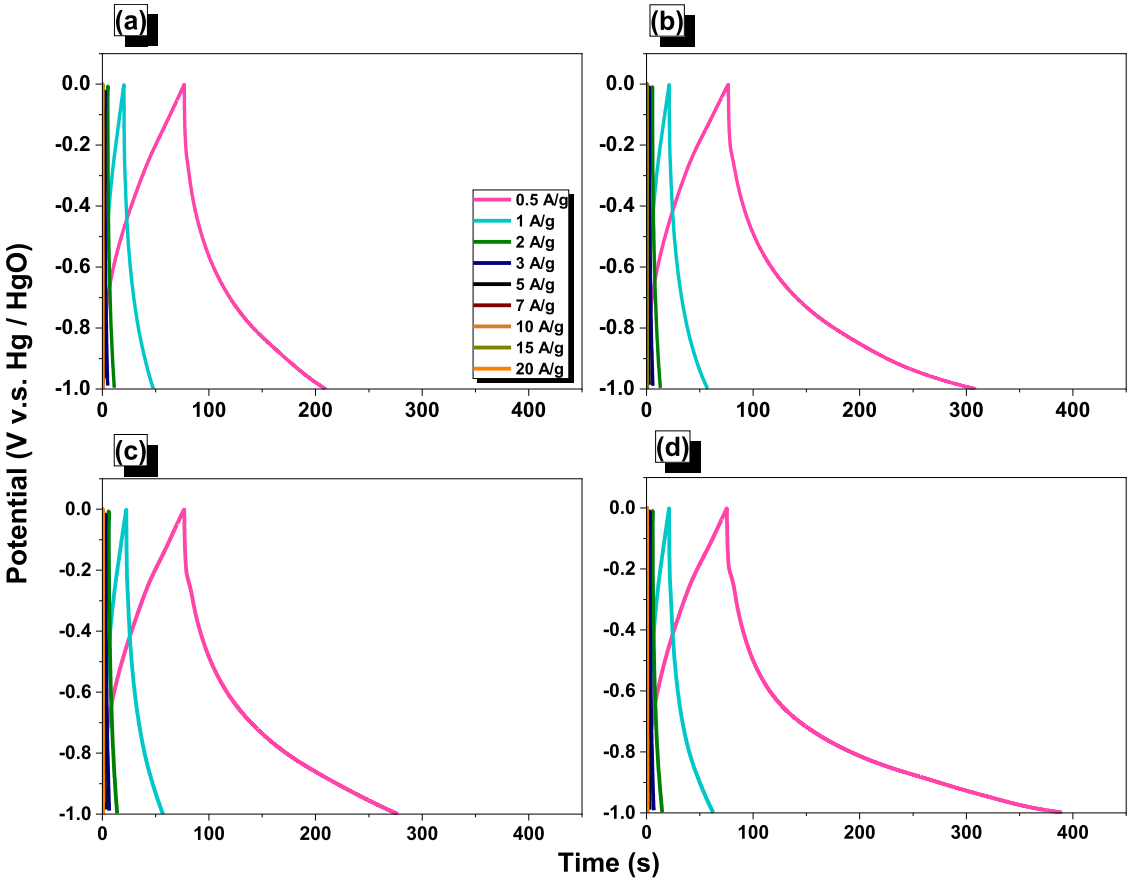

Figure 8. (a–d) GCD curves of the (a) Try-PyT, (b) Try-PyT-BT, (c) Try-TPET, and (d) Try-TPET-BT CMPs.

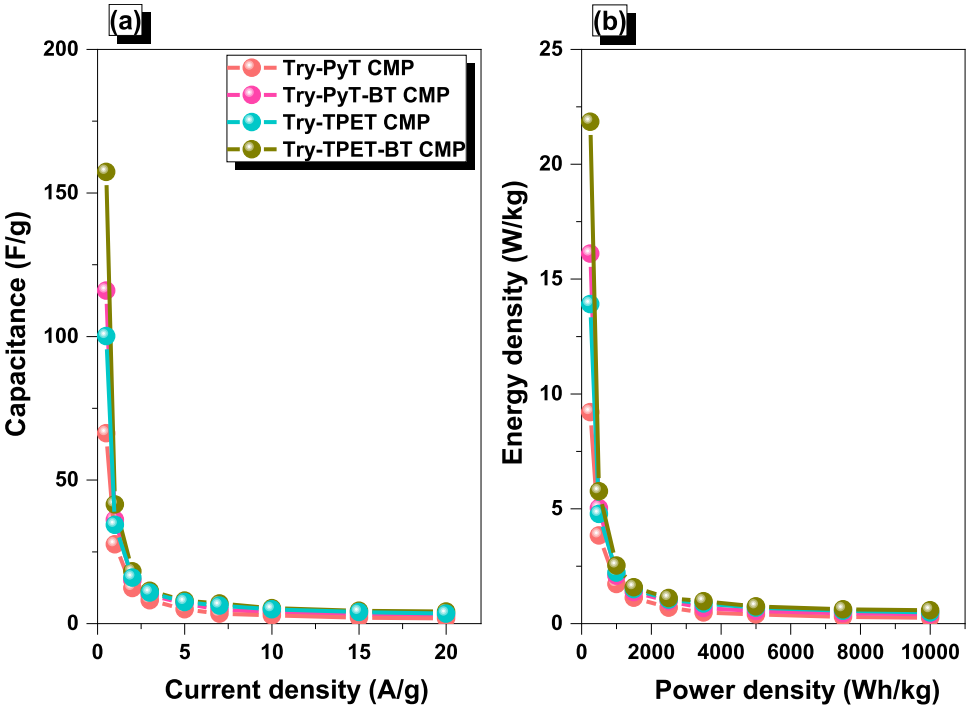

Figure 9. (a) Capacitance performance and (b) Ragone plot of the Try-PyT, Try-PyT-BT, Try-TPET, and Try-TPET-BT CMPs.

g^{-1}. By analyzing the GCD test data, the capacitance values of the different electrodes were calculated.

For Try-PyT, Try-PyT-BT, Try-TPET, and Try-TPET-BT CMPs, the maximum capacitance was observed at a current density of 0.5 A g^{-1}, with values of 66, 116, 100, and 157 F g^{-1}, respectively (Figure 9a). Notably, the CMP containing 1,3-benzothiadiazole (BT) exhibited higher capacitance at every current density, despite having a lower surface area as indicated

https://doi.org/10.1021/acsaem.3c01933
ACS Appl. Energy Mater. 2023, 6, 9012−9024

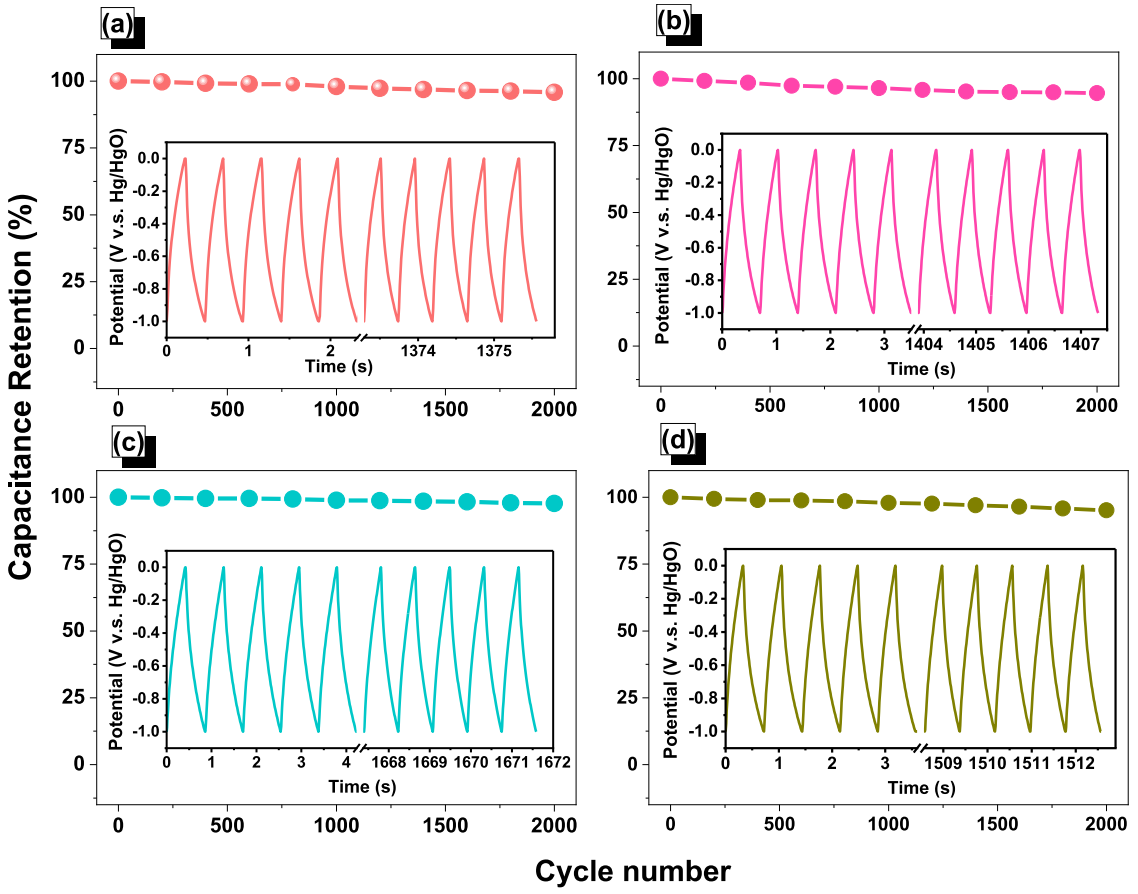

Figure 10. (a–d) Capacitance retention of the (a) Try-PyT, (b) Try-PyT-BT, (c) Try-TPET, and (d) Try-TPET-BT CMPs.

by the BET analysis. The incorporation of nitrogen-rich polymers with conjugated skeletons in supercapacitors has been found to enhance their electrochemical properties, particularly in high-surface-area polymers. Polymers with porous structures provide an extensive surface area, creating numerous active sites for charge storage, while the conjugated skeleton enhances electrical conductivity by promoting electron delocalization. The supercapacitor's total electrochemical performance is enhanced by the quicker electron transport made possible by the greater conductivity. Furthermore, the presence of pseudocapacitive sites in the nitrogen-rich structure of these polymers is essential for improving their electrochemical characteristics.[69,70] These nitrogen-doping sites experience reversible redox reactions, which increase the supercapacitor's total capacitance and energy density. These CMPs display outstanding electrochemical capabilities due to their large surface area, conjugated structure, and nitrogen doping. These Try-based CMPs show a lot of potential for cutting-edge supercapacitor applications due to their high capacitance, outstanding rate capability, and longer cycle stability. They provide a number of benefits and point the way toward the creation of high-performance supercapacitor materials. A Ragone plot was constructed to compare the power density versus energy density for different supercapacitor electrode materials, and Figure 9b illustrates that the Try-TPET-BT CMP exhibits the highest energy density, reaching up to 22 Wh kg^{-1} within the potential range of 1.0 V. This finding highlights the potential of Try-TPET-BT CMP as a promising material for supercapacitor devices. Since the primary objective of this work is to provide a supercapacitor electrode material, it is crucial to consider good capacitance retention and stability over extended periods.

To assess this, stability and capacitance retention were evaluated after subjecting Try-PyT, Try-PyT-BT, Try-TPET, and Try-TPET-BT CMPs to 2000 GCD cycles, as demonstrated in Figure 10a–d. The results indicate that the capacitance retention after the cycling test remains high with values of 95, 94, 97, and 95%, respectively, for the four CMPs. The observed durability and stability of the polymer network composite, particularly the Try-TPET-BT CMP, in KOH electrolyte conditions without pulverizing or swelling are significant advantages. Despite a slight decrease in capacitance retention due to the combination of two monomers in the CMP composite, the overall performance remains commendable. Comparing these results with other porous organic polymers, as summarized in Table S1, it is evident that Try-TPET-BT CMP exhibits better performance, making it a promising candidate for practical supercapacitor applications.

In addition to this, electrochemical impedance spectroscopy (EIS) was used further to study the electrochemical characteristics of these porous materials. EIS is useful to understand its impedance as a function of frequency as well as other electrochemical characteristics, such as capacitance and resistance. The Nyquist plots for Try-PyT and Try-PyT-BT, as well as for Try-TPET and Try-TPET-BT CMPs, are shown in Figure 11a,b, respectively, before and after fitting. The series resistances of the Try-PyT, Try-PyT-BT, Try-TPET, and Try-TPET-BT CMPs were calculated from the EIS data as 14.32, 10, 18.87, and 19.9 Ω, respectively. These series resistances were nearly identical, indicating similar electrochemical

https://doi.org/10.1021/acsaem.3c01933
ACS Appl. Energy Mater. 2023, 6, 9012–9024

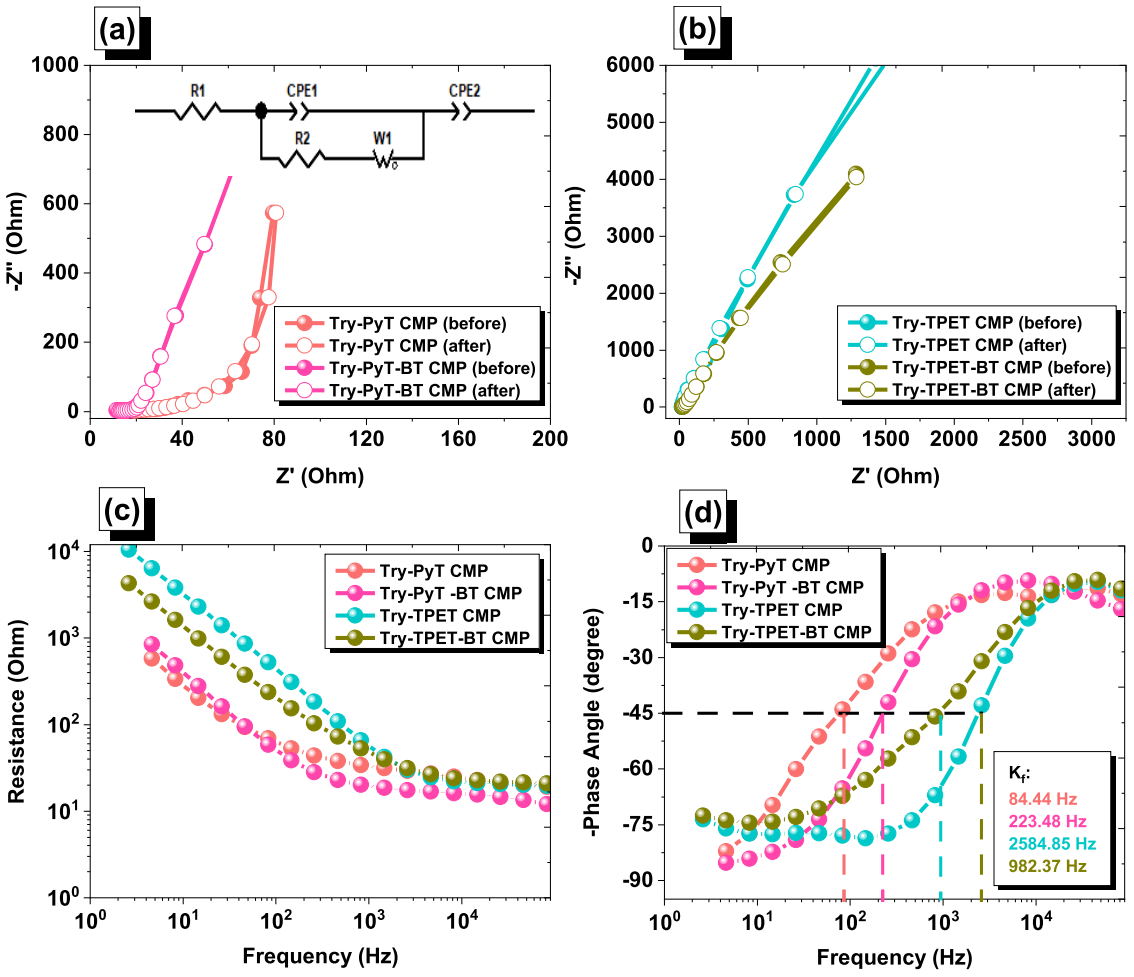

Figure 11. Nyquist plots of (a) Try-PyT and Try-PyT-BT and (b) Try-TPET and Try-TPET-BT CMPs before and after fitting. (c) Bode plots of frequency-dependent resistance (magnitude). (d) Bode plots of frequency-dependent phase angles for Try-PyT and Try-PyT-BT, Try-TPET, and Try-TPET-BT CMPs.

reactions occurring at the surfaces of these electrode materials. Nevertheless, a noticeable difference was seen in the charge transfer resistances of these electrodes. Try-PyT, Try-PyT-BT, Try-TPET, and Try-TPET-BT CMPs exhibited charge transfer resistances of 133.2, 71.37, 7795, and 41.43 Ω, respectively. Try-TPET-BT CMP is shown to have the lowest charge transfer resistance of all of the electrodes, making it the most conductive of the four CMPs. The frequency-dependent magnitude Bode plots are shown in Figure 11c, where they show negative slopes at low frequencies and significant resistance at higher frequencies. Considering that all of these porous materials may be employed as electrode materials for energy storage applications, it is possible that they all exhibit extraordinary capacitive behavior. The frequency-dependent phase-angle Bode graphs for the porous electrodes are displayed in Figure 11d. These figures clearly depict the knee frequencies, which represent the electrode material's rate performance. When the phase angle approaches 45°, the knee frequency occurs, denoting an equal proportion of capacitive and resistive behaviors. For Try-PyT, Try-PyT-BT, Try-TPET, and Try-TPET-BT CMPs, the knee frequencies were found to be 81.44, 223.48, 2584.85, and 982.37 Hz, respectively. Conclusively, all of the electrodes showed significant knee frequencies, showing their potential as electrode materials for energy storage. The EIS suggests that all of these porous materials possess comparable electrochemical properties, especially Try-TPET-BT CMP, which displayed the lowest charge transfer resistance with enhanced rate performance.

CONCLUSIONS

We successfully synthesized four Try-based CMPs using a one-step Sonogashira coupling reaction with PyT, TPET, and BT-Br_2 units. These CMPs exhibited exceptional thermal stability and porosity properties. Notably, the Try-PyT CMP displayed an impressive surface area of 613 m^2 g^{-1}, surpassing those of all other CMPs. On the other hand, the Try-TPET CMP demonstrated the highest thermal stability, achieving a char yield of 70 wt % and a T_{d10} value close to 400 °C. Regarding electrochemical properties, the highest capacitance values were observed at 0.5 A g^{-1} for each CMP: 66 F g^{-1} for Try-PyT, 116 F g^{-1} for Try-PyT-BT, 100 F g^{-1} for Try-TPET, and an impressive 157 F g^{-1} for Try-TPET-BT. These results indicate that the overall performance of these porous Try-CMPs is strongly linked to their surface area. Surprisingly, a notable shift was observed in the connection between the BET surface area and electrochemical performance. This suggests that the impact of heteroatoms becomes the primary influencer on the electrochemical characteristics of these substances. In their role as energy storage components, these electrode materials exhibited exceptional capacity preservation and remained

https://doi.org/10.1021/acsaem.3c01933
ACS Appl. Energy Mater. 2023, 6, 9012−9024

thermally stable throughout 2000 charge−discharge cycles. These results underscore the promise of Try-based CMPs as exceptional materials for energy storage in supercapacitors, indicating a positive outlook for their real-world utilization.

■ ASSOCIATED CONTENT

Supporting Information

The Supporting Information is available free of charge at https://pubs.acs.org/doi/10.1021/acsaem.3c01933.

Details about characterization methods; schematic schemes for the synthesized monomers and Try-CMPs; FTIR and NMR profiles of the synthesized monomers; and SEM-EDS mapping for each CMP (PDF)

■ AUTHOR INFORMATION

Corresponding Authors

Mohamed Gamal Mohamed − *Department of Materials and Optoelectronic Science, College of Semiconductor and Advanced Technology Research, Center for Functional Polymers and Supramolecular Materials, National Sun Yat-Sen University, Kaohsiung 804, Taiwan; Chemistry Department, Faculty of Science, Assiut University, Assiut 71515, Egypt;* orcid.org/0000-0003-0301-8372; Email: mgamal.eldin12@yahoo.com

Shiao-Wei Kuo − *Department of Materials and Optoelectronic Science, College of Semiconductor and Advanced Technology Research, Center for Functional Polymers and Supramolecular Materials, National Sun Yat-Sen University, Kaohsiung 804, Taiwan; Department of Medicinal and Applied Chemistry, Kaohsiung Medical University, Kaohsiung 807, Taiwan;* orcid.org/0000-0002-4306-7171; Email: kuosw@faculty.nsysu.edu.tw

Authors

Tzu-Hsin Weng − *Department of Materials and Optoelectronic Science, College of Semiconductor and Advanced Technology Research, Center for Functional Polymers and Supramolecular Materials, National Sun Yat-Sen University, Kaohsiung 804, Taiwan*

Santosh U. Sharma − *Department of Chemistry, National Sun Yat-Sen University, Kaohsiung 80424, Taiwan; International PhD Program for Science, National Sun Yat-sen University, Kaohsiung 80424, Taiwan*

Islam M. A. Mekhemer − *Department of Materials and Optoelectronic Science, College of Semiconductor and Advanced Technology Research, Center for Functional Polymers and Supramolecular Materials, National Sun Yat-Sen University, Kaohsiung 804, Taiwan; Department of Chemical Engineering, National Tsing Hua University, Hsinchu 30013, Taiwan;* orcid.org/0000-0002-0174-6694

Ho-Hsiu Chou − *Department of Chemical Engineering, National Tsing Hua University, Hsinchu 30013, Taiwan;* orcid.org/0000-0003-3777-2277

Complete contact information is available at: https://pubs.acs.org/10.1021/acsaem.3c01933

Notes

The authors declare no competing financial interest.

■ ACKNOWLEDGMENTS

This study was supported financially by the Ministry of Science and Technology, Taiwan, under contracts MOST 111-2223-E-110-004 and 108-2221-E-110-014-MY3. The authors thank the staff at National Sun Yat-sen University for their assistance with the TEM (ID: EM022600) experiments.

■ REFERENCES

(1) Sprick, R. S.; Jiang, J. X.; Bonillo, B.; Ren, S.; Ratvijitvech, T.; Guiglion, P.; Zwijnenburg, M. A.; Adams, D. J.; Cooper, A. I. Tunable Organic Photocatalysts for Visible-Light-Driven Hydrogen Evolution. *J. Am. Chem. Soc.* **2015**, *137*, 3265−3270.

(2) Das, S.; Heasman, P.; Ben, T.; Qiu, S. Porous organic materials: strategic design and structure-function correlation. *Chem. Rev.* **2017**, *117*, 1515−1563.

(3) Shi, X.; Zhang, Z.; Wei, M.; Wang, X.; Wang, J.; Zhang, Y.; Wang, Y. Three-Dimensional Covalent Organic Framework Membranes: Synthesis by Oligomer Interfacial Ripening and Application in Precise Separations. *Macromolecules* **2022**, *55*, 3259−3266.

(4) Zhang, Y.; Zhang, L.; Zhang, X.; Yang, D.; Du, C.; Wan, L.; Au, C.; Chen, J.; Xie, M. Pyridine-based hypercrosslinked polymers as support materials for palladium photocatalysts and their application in Suzuki−Miyaura coupling reactions. *New J. Chem.* **2020**, *44*, 15202−15208.

(5) Abid, A.; Razzaque, S.; Hussain, I.; Tan, B. Eco-Friendly Phosphorus and Nitrogen-Rich Inorganic−Organic Hybrid Hypercross-linked Porous Polymers via a Low-Cost Strategy. *Macromolecules* **2021**, *54*, 5848−5855.

(6) Côté, A. P.; Benin, A. I.; Ockwig, N. W.; O'Keeffe, M.; Matzger, A. I.; Yaghi, O. M. Porous, Crystalline, Covalent Organic Frameworks. *Science* **2005**, *310*, 1166−1170.

(7) Mohamed, M. G.; Chen, T. C.; Kuo, S. W. Solid-State Chemical Transformations to Enhance Gas Capture in Benzoxazine-Linked Conjugated Microporous Polymers. *Macromolecules* **2021**, *54*, 5866−5877, DOI: 10.1021/acs.macromol.1c00736.

(8) Weng, T. H.; Mohamed, M. G.; Sharma, S. U.; Chaganti, S. V.; Samy, M. M.; Lee, J. T.; Kuo, S. W. Ultrastable Three-Dimensional Triptycene- and Tetraphenylethene-Conjugated Microporous Polymers for Energy Storage. *ACS Appl. Energy Mater.* **2022**, *5*, 14239−14249, DOI: 10.1021/acsaem.2c02809.

(9) Mohamed, M. G.; Hu, H. Y.; Madhu, M.; Samy, M. M.; Mekhemer, I. M. A.; Tseng, W. L.; Chou, H. H.; Kuo, S. W. Ultrastable two-dimensional fluorescent conjugated microporous polymers containing pyrene and fluorene units for metal ion sensing and energy storage. *Eur. Polym. J.* **2023**, *189*, No. 111980, DOI: 10.1016/j.eurpolymj.2023.111980.

(10) Mohamed, M. G.; Samy, M. M.; Mansoure, T. H.; Li, C. J.; Li, W. C.; Chen, J. H.; Zhang, K.; Kuo, S. W. Microporous Carbon and Carbon/Metal Composite Materials Derived from Bio-Benzoxazine-Linked Precursor for CO_2 Capture and Energy Storage Applications. *Int. J. Mol. Sci.* **2022**, *23*, 347 DOI: 10.3390/ijms23010347.

(11) Ejaz, M.; Mohamed, M. G.; Kuo, S. W. Solid-state chemical transformation provides a fully benzoxazine-linked porous organic polymer displaying enhanced CO_2 capture and supercapacitor performance. *Polym. Chem.* **2023**, *14*, 2494−2509, DOI: 10.1039/D3PY00158J.

(12) Mohamed, M. G.; Elsayed, M. H.; Elewa, A. M.; El-Mahdy, A. F. M.; Yang, C. H.; Mohammed, A. A. K.; Chou, H. H.; Kuo, S. W. Pyrene-Containing Conjugated Organic Microporous Polymers for Photocatalytic Hydrogen Evolution from Water. *Catal. Sci. Technol.* **2021**, *11*, 2229−2241.

(13) Mohamed, M. G.; Chaganti, S. V.; Li, M. S.; Samy, M. M.; Sharma, S. U.; Lee, J. T.; Elsayed, M. H.; Chou, H. H.; Kuo, S. W. Ultrastable Porous Organic Polymers Containing Thianthrene and Pyrene Units as Organic Electrode Materials for Supercapacitors. *ACS Appl. Energy Mater.* **2022**, *5*, 6442−6452, DOI: 10.1021/acsaem.2c00942.

(14) Samy, M. M.; Mohamed, M. G.; Mansoure, T. H.; Meng, T. S.; Khan, M. A. R.; Liaw, C. C.; Kuo, S. W. Solid state chemical transformations through ring-opening polymerization of ferrocene-based conjugated microporous polymers in host−guest complexes with benzoxazine-linked cyclodextrin. *J. Taiwan Inst. Chem. Eng.* **2022**, *132*, No. 104110, DOI: 10.1016/j.jtice.2021.10.010.
(15) Singh, P. N.; Mohamed, M. G.; Chaganti, S. V.; Sharma, S. U.; Ejaz, M.; Lee, J. T.; Kuo, S. W. Rational Design of Ultrastable Conjugated Microporous Polymers based on Pyrene and Perylene Units as High-Performance Organic Electrode Materials for Supercapacitor Applications. *ACS Appl. Energy Mater.* **2023**, *6*, 8277−8287, DOI: 10.1021/acsaem.3c01391.
(16) Amin, K.; Ashraf, N.; Mao, L.; Faul, C. F. J.; Wei, Z. Conjugated microporous polymers for energy storage: Recent progress and challenges. *Nano Energy* **2021**, *85*, No. 105958.
(17) Samy, M. M.; Sharma, S. U.; Mohamed, M. G.; Mohammed, A. A. K.; Chaganti, S. V.; Lee, J. T.; Kuo, S. W. conjugated microporous polymers containing ferrocene units for high carbon dioxide uptake and energy storage. *Mater. Chem. Phys.* **2022**, *287*, No. 126177.
(18) Shu, L.; Yu, J.; Cui, Y.; Ma, Y.; Li, Y.; Gao, B.; Wang, H.-G. Porphyrin-based conjugated microporous polymers with dual active sites as anode materials for lithium-organic batteries. *Int. J. Hydrogen Energy* **2022**, *47*, 10902−10910.
(19) Yuan, Y.; Zhu, G. Porous aromatic frameworks as a platform for multifunctional applications. *ACS Cent. Sci.* **2019**, *5*, 409−418.
(20) Mohamed, M. G.; EL-Mahdy, A. F. M.; Kotp, M. G.; Kuo, S. W. Advances in porous organic polymers: syntheses, structures, and diverse applications. *Mater. Adv.* **2022**, *3*, 707−733.
(21) Ejaz, M.; Samy, M. M.; Ye, Y.; Kuo, S. W.; Mohamed, M. G. Design Hybrid Porous Organic/Inorganic Polymers Containing Polyhedral Oligomeric Silsesquioxane/Pyrene/Anthracene Moieties as a High-Performance Electrode for Supercapacitor. *Int. J. Mol. Sci.* **2023**, *24*, 2501 DOI: 10.3390/ijms24032501.
(22) Samy, M. M.; Mohamed, M. G.; Sharma, S. U.; Chaganti, S. V.; Lee, J. T.; Kuo, S. W. An Ultrastable Tetrabenzonaphthalene-Linked conjugated microporous polymer functioning as a high-performance electrode for supercapacitors. *J. Taiwan Inst. Chem. Eng.* **2023**, No. 104750, DOI: 10.1016/j.jtice.2023.104750.
(23) Samy, M. M.; Mohamed, M. G.; Sharma, S. U.; Chaganti, S. V.; Mansoure, T. H.; Lee, J. T.; Chen, T.; Kuo, S. W. Constructing conjugated microporous polymers containing triphenylamine moieties for high-performance capacitive energy storage. *Polymer* **2023**, *264*, No. 125541, DOI: 10.1016/j.polymer.2022.125541.
(24) Mohamed, M. G.; Elsayed, M. H.; Ye, Y.; Samy, M. M.; Hassan, A. E.; Mansoure, T. H.; Wen, Z.; Chou, H.-H.; Chen, K.-H.; Kuo, S.-W. Construction of Porous Organic/Inorganic Hybrid Polymers Based on Polyhedral Oligomeric Silsesquioxane for Energy Storage and Hydrogen Production from Water. *Polymers* **2023**, *15*, 182 DOI: 10.3390/polym15010182.
(25) Mohamed, M. G.; Ahmed, M. M. M.; Du, W.-T.; Kuo, S.-W. Meso/Microporous Carbons from Conjugated Hyper-Crosslinked Polymers Based on Tetraphenylethene for High-Performance CO_2 Capture and Supercapacitor. *Molecules* **2021**, *26*, 738 DOI: 10.3390/molecules26030738.
(26) Lee, J.-S. M.; Cooper, A. I. Advances in Conjugated Microporous Polymers. *Chem. Rev.* **2020**, *120*, 2171−2214.
(27) Gamal Mohamed, M.; Tsai, M.-Y.; Wang, C.-F.; Huang, C.-F.; Danko, M.; Dai, L.; Chen, T.; Kuo, S.-W. Multifunctional Polyhedral Oligomeric Silsesquioxane (POSS) Based Hybrid Porous Materials for CO_2 Uptake and Iodine Adsorption. *Polymers* **2021**, *13*, 221 DOI: 10.3390/polym13020221.
(28) Samy, M. M.; Mekhemer, I. M.; Mohamed, M. G.; Elsayed, M. H.; Lin, K. H.; Chen, Y. K.; Wu, T. L.; Chou, H. H.; Kuo, S. W. Conjugated microporous polymers incorporating Thiazolo[5,4-d]-thiazole moieties for Sunlight-Driven hydrogen production from water. *Chem. Eng. J.* **2022**, *446*, No. 137158, DOI: 10.1016/j.cej.2022.137158.
(29) Mohamed, M. G.; Sharma, S. U.; Liu, N. Y.; Mansoure, T. H.; Samy, M. M.; Chaganti, S. V.; Chang, Y. L.; Lee, J. T.; Kuo, S. W. Ultrastable Covalent Triazine Organic Framework Based on Anthracene Moiety as Platform for High-Performance Carbon Dioxide Adsorption and Supercapacitors. *Int. J. Mol. Sci.* **2022**, *23*, 3174 DOI: 10.3390/ijms23063174.
(30) Zhang, W.; Zuo, H.; Cheng, Z.; Shi, Y.; Guo, Z.; Meng, N.; Thomas, A.; Liao, Y. Macroscale Conjugated Microporous Polymers: Controlling Versatile Functionalities Over Several Dimensions. *Adv. Mater.* **2022**, *34*, No. 2104952.
(31) Lee, J.-S. M.; Wu, T.-H.; Alston, B. M.; Briggs, M. E.; Hasell, T.; Hu, C.-C.; Cooper, A. I. Porosity-Engineered Carbons for Supercapacitive Energy Storage Using Conjugated Microporous Polymer Precursors. *J. Mater. Chem. A* **2016**, *4*, 7665−7673.
(32) Samy, M. M.; Mohamed, M. G.; Kuo, S. W. Conjugated Microporous Polymers Based on Ferrocene Units as Highly Efficient Electrodes for Energy Storage. *Polymers* **2023**, *15*, 1095 DOI: 10.3390/polym15051095.
(33) Mohamed, M. G.; Atayde, E. C.; Matsagar, B. M.; Na, J.; Yamauchi, Y.; Wu, K. C. W.; Kuo, S.-W. Construction Hierarchically Mesoporous/Microporous Materials Based on Block Copolymer and Covalent Organic Framework. *J. Taiwan Inst. Chem. Eng.* **2020**, *112*, 180−192, DOI: 10.1016/j.jtice.2020.06.013.
(34) Bartlett, P. D.; Ryan, M. J.; Cohen, S. G. Triptycene (9,10-o-Benzenoanthracene). *J. Am. Chem. Soc.* **1942**, *64*, 2649−2653.
(35) Ansari, M.; Hassan, A.; Alam, A.; Das, N. A mesoporous polymer bearing 3D-Triptycene, − OH and azo- functionalities: Reversible and efficient capture of carbon dioxide and iodine vapor. *Microporous Mesoporous Mater.* **2021**, *323*, No. 111242.
(36) Hassan, A.; Saritha, C.; Rajana, V. K.; Mandal, D.; Das, N. Rationally Designed Ionic Covalent Organic Networks (iCONs) with Efficient Antimicrobial Activities. *ACS Macro Lett.* **2023**, *12*, 376−381.
(37) Ansari, M.; Alam, A.; Bera, R.; Hassan, A.; Goswami, S.; Das, N. Synthesis, characterization and adsorption studies of a novel triptycene based hydroxyl azo- nanoporous polymer for environmental remediation. *J. Environ. Chem. Eng.* **2020**, *8*, No. 103558.
(38) Alam, A.; Hassan, A.; Bera, R.; Das, N. Silsesquioxane-based and triptycene-linked nanoporous polymers (STNPs) with a high surface area for CO_2 uptake and efficient dye removal applications. *Mater. Adv.* **2020**, *1*, 3406−3416.
(39) Shi, Y. M.; Hu, K.; Cui, Y. X.; Cheng, J. M.; Zhao, W. J.; Li, X. M. Magnetic Triptycene-Based Covalent Triazine Frameworks for The Efficient Extraction of Anthraquinones in Slimming Tea Followed by UHPLC-FLD Detection. *Microchem. J.* **2019**, *146*, 525−533.
(40) Yu, C.; Li, H.; Wang, Y.; Suo, J.; Guan, X.; Wang, R.; Valtchev, V.; Yan, Y.; Qiu, S.; Fang, Q. Three-Dimensional Triptycene-Functionalized Covalent Organic Frameworks with hea Net for Hydrogen Adsorption. *Angew. Chem., Int. Ed.* **2022**, *61*, No. e202117101.
(41) Zhang, C.; Zhu, P.-C.; Tan, L.; Liu, J.-M.; Tan, B.; Yang, X.-L.; Xu, H.-B. Triptycene-Based Hyper-Cross-Linked Polymer Sponge for Gas Storage and Water Treatment. *Macromolecules* **2015**, *48*, 8509−8514.
(42) Dang, Q.-Q.; Wang, X.-M.; Zhan, Y.-F.; Zhang, X.-M. An azo-linked porous triptycene network as an absorbent for CO_2 and iodine uptake. *Polym. Chem.* **2016**, *7*, 643−647.
(43) Mohamed, M. G.; Chang, S.-Y.; Ejaz, M.; Samy, M. M.; Mousa, A. O.; Kuo, S.-W. Design and Synthesis of Bisulfone-Linked Two-Dimensional Conjugated Microporous Polymers for CO_2 Adsorption and Energy Storage. *Molecules* **2023**, *28*, 3234 DOI: 10.3390/molecules28073234.
(44) Ghanem, B. S.; Msayid, K. J.; Mckeown, N. B.; Harris, K. D.; Pan, Z. G.; Budd, P. M.; Butler, A.; Selbie, J.; Book, D.; Walton, A. A Triptycene-Based Polymer of Intrinsic microposity That Displays Enhanced Surface Area and Hydrogen Adsorption. *Chem. Commun.* **2007**, 67.
(45) Li, H.; Chen, F.; Guan, X.; Li, J.; Li, C.; Tang, B.; Valtchev, V.; Yan, Y.; Qiu, S.; Fang, Q. Three-Dimensional Triptycene-Based

Covalent Organic Frameworks with ceq or acs Topology. *J. Am. Chem. Soc.* **2021**, *143*, 2654−2659.
(46) Lin, X.; Deng, Y. Y.; Zhang, Q.; Han, D.; Fu, Q. Effect of POSS size on the porosity and adsorption performance of hybrid porous polymers. *Macromolecules* **2023**, *56*, 1243−1252.
(47) Lyu, W.; Yan, C.; Chen, Z.; Chen, J.; Zuo, H.; Teng, L.; Liu, H.; Wang, L.; Liao, Y. Spirobifluorene-Based Conjugated Microporous Polymer-Grafted Carbon Nanotubes for Efficient Supercapacitive Energy Storage. *ACS Appl. Energy Mater.* **2022**, *5*, 3706−3714.
(48) Najib, S.; Erdem, E. Current progress achieved in novel materials for supercapacitor electrodes: mini review. *Nanoscale Adv.* **2019**, *1*, 2817−2827.
(49) Li, L.; Lu, F.; Xue, R.; Ma, B.; Li, Q.; Wu, N.; Liu, H.; Yao, W.; Guo, H.; Yang, W. Ultrastable triazine-based covalent organic framework with an interlayer hydrogen bonding for supercapacitor applications. *ACS Appl. Mater. Interfaces* **2019**, *11*, 26355−26363.
(50) Xu, Z.; Sun, S.; Han, Y.; Wei, Z.; Cheng, Y.; Yin, S.; Cui, W. High-Energy-Density Asymmetric Supercapacitor Based on a Durable and Stable Manganese Molybdate Nanostructure Electrode for Energy Storage Systems. *ACS Appl. Energy Mater.* **2020**, *3*, 5393−5404.
(51) Liu, Y.; Wang, S.; Meng, X.; Ye, Y.; Song, X.; Liang, Z.; Zhao, Y. Molecular Expansion for Constructing Porous Organic Polymers with High Surface Areas and Well-Defined Nanopores. *Angew. Chem., Int. Ed.* **2020**, *59*, 19487−19493.
(52) Xue, X.; Luo, J.; kong, L.; Zhao, J.; Zhang, Y.; Du, H.; Chen, S.; Xie, Y. The Synthesis of Triazine-Thiophene-Thiophene Conjugated Porous Polymers and their Composites with Carbon as Anode Materials in Lithium-ion Batteries. *RSC Adv.* **2021**, *11*, 10688−10698.
(53) Zhang, Q.; Ge, S.; Wang, X.; Sun, H.; Zhu, Z.; Liang, W.; Li, A. Novel Mno/Conjugated Microporous Polymer Derived-Porous Hard Carbon Nanocomposite for Superior Lithium Storage. *RSC Adv.* **2014**, *4*, 41649−41653.
(54) Li, X.-C.; Zhang, Y.; Wang, C.-Y.; Wan, Y.; Lai, W.-Y.; Pang, H.; Huang, W. Redox-Active Triazatruxene-Based Conjugated Microporous Polymers for High-Performance Supercapacitors. *Chem. Sci.* **2017**, *8*, 2959−2965.
(55) Zhang, C.; He, Y.; Mu, P.; Wang, X.; He, Q.; Chen, Y.; Zeng, J.; Wang, F.; Xu, Y.; Jiang, J.-X. Toward High Performance Thiophene-Containing Conjugated Microporous Polymer Anodes for Lithium-Ion Batteries through Structure Design. *Adv. Funct. Mater.* **2018**, *28*, No. 1705432.
(56) Chai, S.; Hu, N.; Han, Y.; Zhang, X.; Yang, Z.; Wei, L.; Wang, L.; Wei, H. The Microwave-Assisted Solvothermal Synthesis of a Novel β-Ketoenamine-Linked Conjugated Microporous Polymer for Supercapacitors. *RSC Adv.* **2016**, *6*, 49425−49428.
(57) Mohamed, M. G.; Sharma, S. U.; Yang, C.-H.; Samy, M. M.; Mohammed, A. A. K.; Chaganti, S. V.; Lee, J.-T.; Kuo, S. W. Anthraquinone-enriched conjugated microporous polymers as organic cathode materials for high-performance lithium-ion batteries. *ACS Appl. Energy Mater.* **2021**, *4*, 14628−14639, DOI: 10.1021/acsaem.1c03270.
(58) Mohamed, M. G.; Chaganti, S. V.; Sharma, S. U.; Samy, M. M.; Ejaz, M.; Lee, J.-T.; Zhang, K.; Kuo, S.-W. Constructing Conjugated Microporous Polymers Containing the Pyrene-4,5,9,10-Tetraone Unit for Energy Storage. *ACS Appl. Energy Mater.* **2022**, *5*, 10130−10140.
(59) Mohamed, M. G.; Kuo, S. W. Crown Ether-Functionalized Polybenzoxazine for Metal Ion Adsorption. *Macromolecules* **2020**, *53*, 2420−2429, DOI: 10.1021/acs.macromol.9b02519.
(60) Mohamed, M. G.; Samy, M. M.; Mansoure, T. H.; Sharma, S. U.; MS Tsai, M. S.; Chen, J. H.; Lee, J. T.; Kuo, S. W. Dispersions of 1,3,4-Oxadiazole-Linked Conjugated Microporous Polymers with Carbon Nanotubes as a High-Performance Electrode for Supercapacitors. *ACS Appl. Energy Mater.* **2022**, *5*, 3677−3688, DOI: 10.1021/acsaem.2c00100.
(61) Mousa, A. O.; Zheng, I. L.; Chuang, C. H.; Chen, C. K.; Kuo, S. W.; Mohamed, M. G. Rational Design of Bifunctional Microporous Organic Polymers Containing Anthracene and Triphenylamine Units for Energy Storage and Biological Applications. *Int. J. Mol. Sci.* **2023**, *24*, 8966 DOI: 10.3390/ijms24108966.
(62) Mohamed, M. G.; Mansoure, T. H.; Samy, M. M.; Takashi, Y.; Mohammed, A. A. K.; Ahamad, T.; Alshehri, S. M.; Kim, J.; Matsagar, B. M.; Wu, K. C.-W.; Kuo, S.-W. Ultrastable Conjugated Microporous Polymers Containing Benzobisthiadiazole and Pyrene Building Blocks for Energy Storage Applications. *Molecules* **2022**, *27*, 2025.
(63) Duan, H.; Li, Y.; Li, Q.; Wang, P.; Liu, X.; Cheng, L.; Yu, Y.; Cao, L. Host-Guest Recognition and Fluorescence of a Tetraphenylethene-Based Octacationic Cage. *Angew. Chem., Int. Ed.* **2020**, *59*, 10101−10110.
(64) Peng, H.-Q.; Zheng, X.; Han, T.; Kwok, R. T. K.; Lam, J. W. Y.; Huang, X.; Tang, B. Z. Dramatic Differences in Aggregation-Induced Emission and Supramolecular Polymerizability of Tetraphenylethene-Based Stereoisomers. *J. Am. Chem. Soc.* **2017**, *139*, 10150−10156.
(65) Kinik, F. P.; Ortega-Guerrero, A.; Ongari, D.; Ireland, C. P.; Smit, B. Pyrene-based metal organic frameworks: From synthesis to applications. *Chem. Soc. Rev.* **2021**, *50*, 3143−3177.
(66) Qin, J.-H.; Zhang, J.-R.; Xiao, Z.; Wu, Y.-P.; Xu, H.-M.; Yang, X.-G.; Ma, L.-F.; Li, D.-S. Topology- and guest-dependent photoelectric conversion of 2d anionic pyrene-based metal−organic framework. *Cryst. Growth Des.* **2022**, *22*, 4018−4024.
(67) Qin, J.-H.; Huang, Y.-D.; Zhao, Y.; Yang, X.-G.; Li, F.-F.; Wang, C.; Ma, L.-F. Highly dense packing of chromophoric linkers achievable in a pyrene-based metal-organic framework for photoelectric response. *Inorg. Chem.* **2019**, *58*, 15013−15016.
(68) Chinchilla, R.; Najera, C. Recent Advances in Sonogashira Reactions. *Chem. Soc. Rev.* **2011**, *40*, 5084−5512.
(69) Gang, X.; Krishnamoorthy, M.; Jiang, W.; Pan, J.; Pan, Z.; Liu, X. A novel in-situ preparation of N-rich spherical porous carbon as greatly enhanced material for high-performance supercapacitors. *Carbon* **2021**, *171*, 62−71.
(70) Zheng, L.; Tang, B.; Dai, X.; Xing, T.; Ouyang, Y.; Wang, Y.; Chang, B.; Shu, H.; Wang, X. High-yield synthesis of N-rich polymer-derived porous carbon with nanorod-like structure and ultrahigh N-doped content for high-performance supercapacitors. *Chem. Eng. J.* **2020**, *399*, No. 125671.